

# An Analysis of the Exponential Electric Displacement Saturation Model in Fracturing Piezoelectric Ceramics

C. Linder

*This paper presents a numerical analysis of a recently proposed exponential electric displacement saturation model to simulate crack initiation and crack propagation in piezoelectric ceramics. The motivation for the account of electric displacement saturation on a constitutive level can be found in the observed difference between theoretical predictions and the actual experimental obtained dependency of crack propagation onset on the applied electric field. Contrary to earlier accounts of electric displacement saturation, the exponential saturation of the electric displacement versus electric field relation allows for applications in problems like propagating cracks in fracturing piezoelectric ceramics where no analytical solutions exist. This requires the incorporation of strong discontinuities in the form of jumps in the displacement field and the electric potential for the electromechanical coupled solid within the individual finite elements. Based on two numerical examples for which experimental results are available the extension of such an advanced finite element framework to take into account electric displacement saturation is shown in this work to be independent of the finite element discretization and results in numerical solutions close to the experimentally observed results.*

## 1 Introduction

Two major challenges arise when numerically modeling piezoelectric ceramics at failure. First, the electromechanical coupled material requires a sophisticated constitutive model to describe realistically appearing physical phenomena like anisotropy, the direct and converse piezoelectric effect or the observed polarization switching for alternating applied electric fields. Secondly, the numerical description of failure, which already poses a challenge in purely mechanical materials and gains complexity for electromechanical coupled materials, requires advanced computational frameworks to describe the appearing physical phenomena like cracks for which criteria of initiation and propagation are needed in an efficient way. The particular material modeled in this work is an already poled lead zirconate titanate PZT-4 piezoelectric ceramics operated in a regime where polarization switching is assumed to not play a role. Due to its high brittleness characterized by a fracture toughness in the order  $1 \text{ MPa}\sqrt{\text{m}}$  (Suo et al., 1992) such material is though prone to fracture and therefore an ideal candidate to investigate the effect of electric displacement saturation.

This saturation of the electric displacement for large electric fields can be motivated by physical arguments for piezoelectric ceramics showing a reduction of the ionic movement in such materials at high applied electric fields (Jona and Shirane, 1993) and in that way poses a limitation on the amount of the polarization and hence the electric displacement. Since in electromechanical coupled materials defects in the form of inhomogeneities, voids or cracks not only are causing a drastic amplification of stresses but also result in a drastic increase of the electric quantities, those regions are identified as possible areas where electric displacement saturation might play a key role. In particular, it led to the development of a *strip saturation model* in Gao et al. (1997) with the goal to explain the discrepancies between the experimentally observed results and the theoretical predicted influence of the electric field on the initiation of crack growth in an infinite domain including a pre-existing notch. Whereas the energy release rate, a key fracture quantity whose value is a measure of potential crack initiation which can be theoretically computed through complex variable approaches extended from mechanical problems (Lekhnitskii, 1950; Eshelby et al., 1953; Stroh, 1958) to the linear piezoelectric regime (Parton, 1976; Pak, 1990; Suo et al., 1992), predicts an even dependency of the crack initiation on the applied electric field (i.e. regardless of the orientation of the applied electric field with respect to the polarization direction the initiation of cracks perpendicular to the poling direction is always inhibited), experiments report an odd dependency (Tobin and Pak, 1993; Park and Sun, 1995b; Wang and Singh, 1997; Fu and Zhang, 2000). To avoid this discrepancy, in Park and Sun (1995a) the *strain energy release rate* is suggested as a possible fracture criterion which led to theoretical predictions close to experimental

results but also raised criticism due to its lack of physical foundation (Gao et al., 1997; Fulton and Gao, 2001; McMeeking, 2001). Another approach is suggested in Gao et al. (1997) based on the introduction of a new *local energy release rate* which arises when computing a path integral which crosses the introduced saturation zone in front of the crack tip oriented normal to the poling direction and limits the electric displacement to not surpass a certain saturation value. Their approach follows the one of Dugdale (1960) for the incorporation of plasticity into material models of metals and relies on the superposition of a complex function onto the singular solution of a crack in an infinite linear piezoelectric material and therefore is limited to problems for which such analytical solutions exist. For those though, the approach nicely agrees with the tendency observed in experiments.

The deficiency of being restricted to problems for which analytical solutions exist is avoided in a recently proposed simplified account of electric saturation of exponential type in Linder and Miehe (2012). In that work, firstly the effect of displacement saturation is analyzed for unpoled ferroelectric ceramics when no cracks are present by its incorporation into a rate-dependent ferroelectric model proposed in Miehe and Rosato (2011) resulting in a modification of the dielectric hysteresis curves in the region of high electric fields. Secondly, the exponential electric displacement saturation model is also incorporated into an advanced finite element formulation capable of describing strong discontinuities, i.e. jumps in the displacement field and the electric potential, in the interior of the individual finite elements. This allowed for the simulation of two realistic problems in the form of a compact tension test and an off-centered three point bending test of a PZT-4 piezoelectric ceramic material loaded mechanically and electrically so that a crack starts to propagate from a pre-existing notch through the overall specimen. Comparisons of the fracture initiation load and the crack paths with the experimentally observed results in Park and Sun (1995b) revealed an excellent agreement. In particular, the curved crack path observed in experiments for the three point bending test is closely matched contrary to the almost straight crack path predicted in an earlier work (Linder et al., 2011a).

The numerical framework which allows for the numerical modeling of strong discontinuities also employed in this work goes back to the work of Simo et al. (1993). Extensions to two dimensions (Simo and Oliver, 1994; Armero and Garikipati, 1995) and three dimensions (Wells, 2001; Mosler and Meschke, 2003) or to the finite deformation regime (Armero and Garikipati, 1996) within the purely mechanical framework have been made over the years. Following an approach of identifying certain separation modes of the fracture process and incorporating those directly into the finite element formulation (Linder and Armero, 2007, 2009; Armero and Linder, 2008, 2009) an extension to model fracture also in electromechanical coupled solids is proposed in Linder et al. (2011a). Use of a decomposition of the overall problem into a global problem representing the standard electromechanically coupled boundary value problem and a local problem through which the strong discontinuities are incorporated is made. Introduced additional unknowns to describe the amount of displacement separation or the amount of jump in the electric potential can be statically condensed out on the element level resulting in an extremely efficient finite element formulation. This possible static condensation sets this framework apart from nodally enriched approaches (Moës et al., 1999) where the overall size of the system increases with an increase of the crack length. Both methods have in common that in addition to the material model in the bulk additional constitutive relations along the strong discontinuities are needed. Due to the brittleness of the material under investigation, in this work the crack boundary conditions are chosen as mechanically fully softened and electrically impermeable. It is noted though, that in particular the latter assumption is heatedly discussed in the literature (Parton, 1976; Deeg, 1980; Hao and Shen, 1994; Landis, 2004).

The scope of this work is to numerically show that the incorporation of the simplified exponential electric saturation model into the advanced finite element framework capable of describing strong discontinuities in the displacement field and the electric potential yields a formulation which is independent of the finite element discretization. It is shown that the fitted value of an introduced parameter of the saturation model characteristic for the saturation shape is independent of the mesh size, as are the values for the crack initiation onset and the predicted crack paths. Section 2 illustrates the account of electric displacement saturation of exponential type into a standard invariant formulation of anisotropic linear piezoelectricity. The numerical finite element framework with embedded strong discontinuities is briefly reviewed in Section 3 where the required modifications to account for electric displacement saturation are pointed out. Two numerical simulations in the form of the compact tension test and the off-centered three point bending test are performed in Section 4 and compared with the experimentally obtained results in Park and Sun (1995b). The discretization independence of the obtained results is demonstrated based on the comparison of the numerical results for different finite element discretizations. Finally, in Section 5 a few concluding remarks related to this work are given.

## 2 Account of Electric Displacement Saturation in Piezoelectric Ceramics

A piezoelectric solid in  $1 \leq n_{\text{dim}} \leq 3$  dimensions is characterized by the mechanical displacement field  $\mathbf{u}$  and the electric potential  $\varphi$ . From those primary unknowns the symmetric infinitesimal strain tensor  $\boldsymbol{\varepsilon}$  and the electric field  $\mathbf{e}$  follow as

$$\boldsymbol{\varepsilon} = (\text{grad } \mathbf{u})^s = \frac{1}{2}[\text{grad } \mathbf{u} + (\text{grad } \mathbf{u})^T] \quad \text{and} \quad \mathbf{e} = -\text{grad } \varphi \quad (1)$$

where  $\text{grad}(\cdot)$  is the standard gradient operator of a quantity  $(\cdot)$  with respect to the coordinate  $\mathbf{x}$  of a material point. The second law of thermodynamics yields the symmetric stress tensor  $\boldsymbol{\sigma}$  and the electric displacement field  $\mathbf{d}$  based on the electric enthalpy function  $\hat{\psi}$  as

$$\boldsymbol{\sigma} = \partial_{\boldsymbol{\varepsilon}} \hat{\psi}(\boldsymbol{\varepsilon}, \mathbf{e}) \quad \text{and} \quad \mathbf{d} = -\partial_{\mathbf{e}} \hat{\psi}(\boldsymbol{\varepsilon}, \mathbf{e}). \quad (2)$$

Together with the density of free charge carriers  $\rho^e$  and the external volumetric loading  $\rho \mathbf{b}$ , the governing field equations within the body for the infinitesimal theory and the quasi-static case are given as

$$\text{div } \boldsymbol{\sigma} + \rho \mathbf{b} = \mathbf{0} \quad \text{and} \quad \text{div } \mathbf{d} = \rho^e. \quad (3)$$

After separating the overall boundary of the solid into  $\partial\Omega = \overline{\partial_u\Omega} \cup \partial_t\Omega$  and  $\partial\Omega = \overline{\partial_\varphi\Omega} \cup \partial_q\Omega$ , where the displacement and the electric potential are prescribed as  $\mathbf{u} = \bar{\mathbf{u}}$  and  $\varphi = \bar{\varphi}$  on  $\partial_u\Omega$  and  $\partial_\varphi\Omega$ , respectively, and the traction and the surface charge density are imposed as  $\boldsymbol{\sigma} \mathbf{n} = \bar{\mathbf{t}}$  and  $\mathbf{d} \cdot \mathbf{n} = -\bar{q}$  on  $\partial_t\Omega$  and  $\partial_q\Omega$ , respectively, standard arguments yield the weak equations corresponding to the field equations (3) as

$$\int_{\Omega} \rho \mathbf{b} \cdot \delta \mathbf{u} dV + \int_{\partial_t\Omega} \bar{\mathbf{t}} \cdot \delta \mathbf{u} dA - \int_{\Omega} \boldsymbol{\sigma} \cdot (\text{grad } \delta \mathbf{u})^s dV = 0 \quad \text{and} \quad \int_{\Omega} \rho^e \delta \varphi dV + \int_{\partial_q\Omega} \bar{q} \delta \varphi dA + \int_{\Omega} \mathbf{d} \cdot (\text{grad } \delta \varphi) dV = 0 \quad (4)$$

for all admissible variations  $\delta \mathbf{u}$  and  $\delta \varphi$  with  $\delta \mathbf{u} = \mathbf{0}$  on  $\partial_u\Omega$  and  $\delta \varphi = 0$  on  $\partial_\varphi\Omega$ , respectively.

To account for electric displacement saturation, the invariant formulation proposed in Schröder and Gross (2004) to model the response of piezoelectric ceramics with a macroscopic polarization whose director  $\mathbf{a} = \mathbf{p}/|\mathbf{p}|$ , where  $\mathbf{p}$  is the polarization vector, remains constant when operated within a limited linear regime is modified in Linder and Miehe (2012) through an exponential saturation of the relation between the electric displacement field and the electric field as illustrated in the left part of Figure 1. The electric enthalpy function of the resulting linear piezoelectric model is given as

$$\hat{\psi} = \hat{\psi}_1(I_1, I_2, I_3, I_4) + \hat{\psi}_2(I_5, I_6) + \hat{\psi}_3(I_1, I_3, I_5, I_6, I_7) \quad (5)$$

in terms of the purely mechanical contribution  $\hat{\psi}_1$  and the electromechanical coupled part  $\hat{\psi}_3$  given as

$$\hat{\psi}_1 = \frac{1}{2} \lambda I_1^2 + \mu I_2 + \alpha_1 I_4 + \alpha_2 I_3^2 + \alpha_3 I_1 I_3 \quad \text{and} \quad \hat{\psi}_3 = \beta_1 I_1 I_6 + \beta_2 I_3 I_5 + \beta_3 I_7 \quad (6)$$

as well as the purely electrical contribution  $\hat{\psi}_2$  responsible for the electric displacement saturation and given as

$$\hat{\psi}_2 = (\gamma_1 I_5 + \gamma_2 I_6^2) \cdot \exp(-|I_6|/\xi). \quad (7)$$

The used invariants are defined as  $I_1 = \boldsymbol{\varepsilon} \cdot \mathbf{1}$ ,  $I_2 = \boldsymbol{\varepsilon}^2 \cdot \mathbf{1}$ ,  $I_3 = \boldsymbol{\varepsilon} \cdot \mathbf{a} \otimes \mathbf{a}$ ,  $I_4 = \boldsymbol{\varepsilon}^2 \cdot \mathbf{a} \otimes \mathbf{a}$ ,  $I_5 = \mathbf{e} \cdot \mathbf{e}$ ,  $I_6 = \mathbf{e} \cdot \mathbf{a}$  and  $I_7 = \boldsymbol{\varepsilon} \cdot \mathbf{a} \otimes \mathbf{e}$  in terms of the second-order identity tensor  $\mathbf{1}$  and the polarization director  $\mathbf{a}$ . The employed material parameters are  $\lambda$ ,  $\mu$ ,  $\alpha_1$ ,  $\alpha_2$  and  $\alpha_3$  for the elastic constants,  $\beta_1$ ,  $\beta_2$  and  $\beta_3$  for the piezoelectric constants and  $\gamma_1$  and  $\gamma_2$  for the dielectric constants. In addition, the saturation exponent  $\xi$  is introduced in (7) to describe the shape of the electric saturation. Note that  $\xi \rightarrow \infty$  recovers the case when electric displacement saturation is not accounted for. Insertion of the expression (5) for the electric enthalpy into (2) results in closed form solutions of the stresses and the electric displacement field as

$$\begin{aligned} \boldsymbol{\sigma} &= (\lambda I_1 + \alpha_3 I_3 + \beta_1 I_6) \mathbf{1} + 2\mu \boldsymbol{\varepsilon} + 2\alpha_1 (\boldsymbol{\varepsilon} \mathbf{a} \otimes \mathbf{a})^s + (2\alpha_2 I_3 + \alpha_3 I_1 + \beta_2 I_6) (\mathbf{a} \otimes \mathbf{a}) + \beta_3 (\mathbf{e} \otimes \mathbf{a})^s \\ \mathbf{d} &= -\left[ (\beta_1 I_1 + \beta_2 I_3) \mathbf{a} + \beta_3 \boldsymbol{\varepsilon} \mathbf{a} \right] + \left[ -2\gamma_1 \mathbf{e} - 2\gamma_2 I_6 \mathbf{a} + \frac{1}{\xi} \frac{I_6}{|I_6|} (\gamma_1 I_5 + \gamma_2 I_6^2) \mathbf{a} \right] \cdot \exp(-|I_6|/\xi). \end{aligned} \quad (8)$$

The sensitivities of the stresses and the electric displacement with respect to the strain field and the electric field yield the fourth-order elasticity tensor  $\mathbb{C} = \partial_{\boldsymbol{\varepsilon}} \boldsymbol{\sigma}$ , the third-order tensor of piezoelectric moduli  $\mathbb{h} = \partial_{\mathbf{e}} \mathbf{d}$  and the

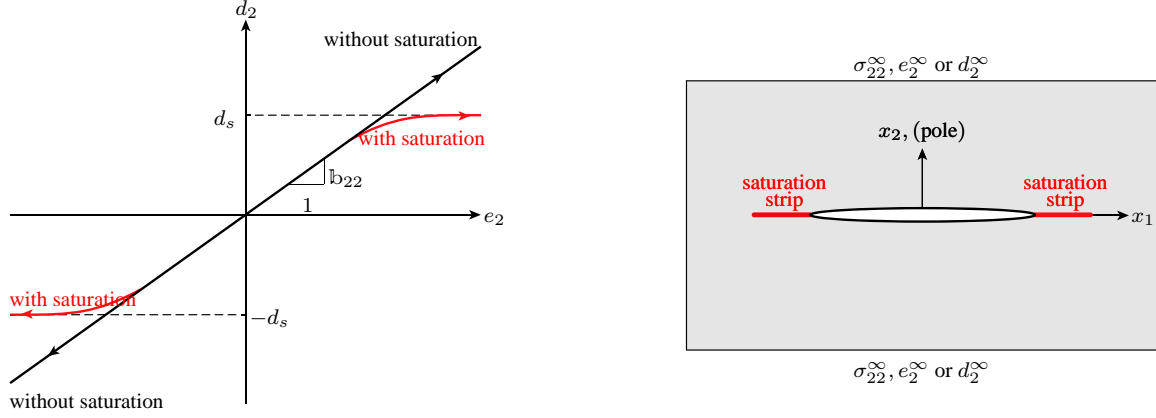


Figure 1: Illustration of the influence of the electric displacement saturation model of exponential type proposed in Linder and Miehe (2012) on the simplified electric displacement versus electric field relation in piezoelectric ceramics (left). Illustration of the strip saturation model proposed in Gao et al. (1997) confined to a strip ahead of the crack tip with saturated electric displacement  $d_2 = d_s$  (right).

second-order tensor of dielectric moduli  $\mathfrak{b} = \partial_e d$ . Of particular interest for the electric saturation model is the closed form expression of the latter given as

$$\mathfrak{b} = \left[ -2\gamma_1 \mathbf{1} - 2\gamma_2 (\mathbf{a} \otimes \mathbf{a}) + \frac{4}{\xi} \frac{I_6}{|I_6|} (\gamma_1 (\mathbf{e} \otimes \mathbf{a})^s + \gamma_2 I_6 (\mathbf{a} \otimes \mathbf{a})) - \frac{1}{\xi^2} (\gamma_1 I_5 + \gamma_2 I_6^2) (\mathbf{a} \otimes \mathbf{a}) \right] \cdot \exp(-|I_6|/\xi) \quad (9)$$

which approaches zero in all components for  $|I_6| \rightarrow \infty$  rather than the constant value  $\mathfrak{b} = -2\gamma_1 \mathbf{1} - 2\gamma_2 (\mathbf{a} \otimes \mathbf{a})$  obtained when no electric displacement saturation is accounted for.

The motivation for the exponential saturation (7) originally introduced in Linder and Miehe (2012) goes back to the work of Gao et al. (1997), who introduced a displacement saturation model along a strip ahead of the crack tip of a piezoelectric material as shown on the right of Figure 1 to resolve the discrepancy between experimental and theoretical results observed along the prediction of the dependency of the crack propagation onset on the applied electric field. The analytical solution derived in Gao et al. (1997) is obtained by the superposition of a complex function to account for the electric displacement saturation onto the singular solution of a piezoelectric crack in an infinite domain, similar to an approach developed by Dugdale (1960) for the modeling of the plastic deformation in a thin metal sheet. The necessity of closed form solutions substantially limits the applicability of such approach. This limitation is avoided in the formulation proposed in Linder and Miehe (2012) by the simplified account for electric displacement saturation based on (7). Closed form expressions of total and strain energy release rates derived by a complex variable solution (Stroh, 1958; Barnett and Lothe, 1975; Suo et al., 1992) of a Mode I and a Mode III crack in an infinite domain when accounting for the exponential electric displacement saturation in Linder and Miehe (2012) revealed a reduced dependency of these values on the orientation of the applied electric field in the presence of electric displacement saturation. The even dependency on the orientation of the electric field for the total energy release rate and the odd dependency of the strain energy release rate is kept though so that for the latter a positive electric field along the polarization direction enhances crack growth whereas a negative electric field, i.e. acting opposite to the polarization direction, impedes crack growth as also observed in experimental results in Park and Sun (1995b). In addition, in Linder and Miehe (2012) the electric displacement saturation model is applied to problems where no analytical solutions exist. Examples include the investigation of its account on a material response proposed in Miehe and Rosato (2011) which is capable of representing dissipative effects in piezoelectric ceramics by a proper account of polarization switching as well as the investigation of its influence when it comes to the numerical solution of crack initiation and crack propagation by a finite element approach which is capable to describe strong discontinuities in the element interior, the so called *finite elements with embedded strong discontinuities*.

It is the goal of this work to show, that the numerical results obtained by this advanced finite element approach in Linder and Miehe (2012) when accounting for electric displacement saturation are independent of the chosen finite element discretization. To do so, in the following Section 3 a brief introduction of the finite element approach with embedded strong discontinuities is given, before in Section 4 the actual numerical investigation of the discretization influence is provided by a comparison of the numerical results obtained for a compact tension test and an off-centered three point bending test of a PZT-4 piezoelectric material.

### 3 Finite Elements with Embedded Strong Discontinuities Accounting for Electric Displacement Saturation

In this section a brief review of the approach capable to embed strong discontinuities within the individual elements is presented and the minor modifications needed for the account of electric displacement saturation are outlined. Section 3.1 shows how strong discontinuities in the form of jumps in the primary unknowns can be embedded into the continuum setting which subsequently is extended towards the finite element setting in Section 3.2.

#### 3.1 Account for Strong Discontinuities and Electric Displacement Saturation in the Continuum Setting

To model failure in solids and describe the phenomena of crack initiation and crack propagation, the setting outlined in Section 2 must be extended. In particular, jumps in the displacement field and the electric potential must be accounted for to model the characteristics of a fracturing piezoelectric solid. The finite element approach with embedded strong discontinuities does this by a decomposition of the overall problem into a *global problem* representing the standard electromechanical coupled boundary value problem without the presence of strong discontinuities and a *local problem* through which those are incorporated into the formulation. Within the continuum setting this means that a material point  $x$  of the global problem is equipped through the local problem with the possibility of forming a strong discontinuity  $\Gamma_x$  separating the local neighborhood  $\Omega_x \subset \Omega$  of the material point into two parts  $\Omega_x^+$  and  $\Omega_x^-$ . As a result, jumps  $[[\mathbf{u}]]$  and  $[[\varphi]]$  in the displacement field and the electric potential arise, where  $[[(\cdot)]] = (\cdot)^+ - (\cdot)^-$ . An illustration of this decomposition is given in Figure 2.

The overall primary variables  $\mathbf{u}$  and  $\varphi$  in  $\Omega_x$  following from this decomposition can then be computed as

$$\mathbf{u} = \mathbf{u}_{\text{global}} + \mathbf{u}_{\text{local}}([[ \mathbf{u} ]]) \quad \text{and} \quad \varphi = \varphi_{\text{global}} + \varphi_{\text{local}}([[ \varphi ]]) \quad (10)$$

where  $\mathbf{u}_{\text{global}}$  and  $\varphi_{\text{global}}$  are the contributions coming from the global problem and  $\mathbf{u}_{\text{local}}([[ \mathbf{u} ]])$  and  $\varphi_{\text{local}}([[ \varphi ]])$  are those arising from the local problem, directly depending on the jumps  $[[ \mathbf{u} ]]$  and  $[[ \varphi ]]$ . The decomposition observed in (10) carries along to the expression for the total strain field  $\boldsymbol{\varepsilon}$  and the total electric field  $\mathbf{e}$ , which after insertion of (10) into (1) take analogous forms as

$$\boldsymbol{\varepsilon} = \boldsymbol{\varepsilon}_{\text{global}}(\mathbf{u}_{\text{global}}) + \boldsymbol{\varepsilon}_{\text{local}}([[ \mathbf{u} ]]) \quad \text{and} \quad \mathbf{e} = \mathbf{e}_{\text{global}}(\varphi_{\text{global}}) + \mathbf{e}_{\text{local}}([[ \varphi ]]) \quad (11)$$

which is valid in the bulk of the neighborhood  $\Omega_x \setminus \Gamma_x$ . As before,  $\boldsymbol{\varepsilon}_{\text{global}}$  and  $\mathbf{e}_{\text{global}}$  are the global quantities arising from the global problem and  $\boldsymbol{\varepsilon}_{\text{local}}$  and  $\mathbf{e}_{\text{local}}$  are the local parts arising from the local problem with a dependency of the latter on the arising jumps  $[[ \mathbf{u} ]]$  and  $[[ \varphi ]]$  in the primary unknowns.

Through the decomposition (10) new unknowns  $[[ \mathbf{u} ]]$  and  $[[ \varphi ]]$  are introduced. Their determination requires additional equations. Those can be physically motivated by the requirement that the traction along the strong discontinuity arising from the stresses in the bulk  $\mathbf{t} = \boldsymbol{\sigma} \mathbf{n}$  must be in equilibrium with the traction  $\hat{\mathbf{t}}([[ \mathbf{u} ]])$  arising from a constitutive model along  $\Gamma_x$  which depend on the actual displacement separation  $[[ \mathbf{u} ]]$ . Similarly, equilibrium must be satisfied between the normal component of the electric displacement field  $q = -\mathbf{d} \cdot \mathbf{n}$  and an applied surface charge density  $\bar{q}$ . The weak form of those requirements can then be stated for the admissible variations  $\delta[[ \mathbf{u} ]]$  and  $\delta[[ \varphi ]]$  as

$$\int_{\Gamma_x} \delta[[ \mathbf{u} ]] \cdot (\boldsymbol{\sigma} \mathbf{n} - \mathbf{t}_\Gamma) dA = 0 \quad \text{and} \quad \int_{\Gamma_x} \delta[[ \varphi ]] (\mathbf{d} \cdot \mathbf{n} + q_\Gamma) dA = 0. \quad (12)$$

The stresses and the electric displacements then follow from the total strain and electric fields in (11) through the constitutive relation (2) depending on a proper choice of the electric enthalpy function  $\hat{\psi}$ . To account for electric displacement saturation use of the expression in (5) for  $\hat{\psi}$  together with the particular choice of the dielectric contribution  $\hat{\psi}_2$  in (7) is made. It can be observed that the way how the strong discontinuity is incorporated through the local problem is not affected by the account for electric displacement saturation.

In addition to the constitutive relation in the bulk, the traction and the surface charge density along the strong discontinuity must be computed based on a constitutive relation along  $\Gamma_x$ . A thermodynamic consistent framework is proposed in Linder et al. (2011a) resulting in a relation of the normal component of traction  $t_{\Gamma_n}$  and the normal component of the displacement jump  $[[u_n]]$  as well as a relation between the surface charge  $q_\Gamma$  and the amount of electric potential jump  $[[\varphi]]$  as

$$t_{\Gamma_n} = \max \{0, f_{t_n} + \mathcal{S}_n[[u_n]]\} \quad \text{and} \quad -q_\Gamma = \frac{[[\varphi]]}{[[[\varphi]]]} \cdot \max \{0, f_\varphi + \mathcal{S}_\varphi[[\varphi]]\}. \quad (13)$$

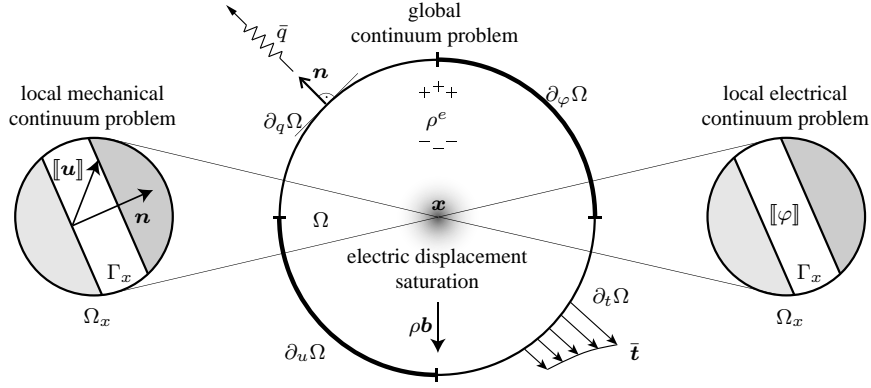


Figure 2: Continuum setting of the finite element approach with embedded strong discontinuities. At a material point  $x$  of the global continuum problem the constitutive relation is taking into account electric displacement saturation and a possible appearance of a strong discontinuity. The latter is accounted for through the local mechanical and electrical problems with possible jumps  $[[u]]$  and  $[[\varphi]]$  in the displacement field and the electric potential.

Here, the strength  $f_{t_n}$  against normal separation, the normal component of the electric displacement  $f_\varphi$  present when the discontinuity is initiated as well as the softening moduli  $\mathcal{S}_n < 0$  and  $\mathcal{S}_\varphi < 0$  of the mechanical and electrical cohesive damage law are introduced.

For the determination of the onset of crack initiation and its propagation direction a common criterion is given by the loss of ellipticity condition. This criterion, commonly used for mechanical problems (Simo et al., 1993; Armero and Garikipati, 1995; Oliver et al., 2003) is extended in Linder et al. (2011a) to electromechanical coupled problems. After its onset, the numerical simulations shown in Section 4 make use of the assumption of fully softened and electrical impermeable crack boundary conditions.

Next, this continuum framework is shown to be easily transferred to the finite element where the global problem now consists of the discretized domain of the specimen and the local problem is replaced by a single finite element which now is capable of having a strong discontinuity propagating through it.

### 3.2 Account for Strong Discontinuities and Electric Displacement Saturation in the Finite Element Setting

In the discrete setting the decomposition of the overall problem into global and local parts introduced within the continuum setting of Section 3.1 is retained. As illustrated in Figure 3, the solid  $\Omega^h = \bigcup_{e=1}^{n_{\text{elem}}} \Omega_e^h$  is discretized by  $n_{\text{elem}}$  finite elements  $\Omega_e^h$ . In the presence of strong discontinuities, this discretization represents the global problem with the required approximation of the global displacement field, the global electric potential, the global strain field and the global electric field as

$$\mathbf{u}_{\text{global}}^h = \mathbf{N}_u \mathbf{d}, \quad \varphi_{\text{global}}^h = \mathbf{N}_\varphi \phi, \quad \boldsymbol{\varepsilon}_{\text{global}}^h = \bar{\mathbf{B}}_u \mathbf{d} \quad \text{and} \quad \mathbf{e}_{\text{global}}^h = -\bar{\mathbf{B}}_\varphi \phi \quad (14)$$

in terms of the standard shape function matrices  $\mathbf{N}_u$  and  $\mathbf{N}_\varphi$ , the generic “B-bar” matrices  $\bar{\mathbf{B}}_u$  and  $\bar{\mathbf{B}}_\varphi$  for standard displacement based, mixed, or enhanced finite element formulations as well as the nodal values  $\mathbf{d}$  and  $\phi$  of displacements and the electric potential. Insertion of the approximations (14) into the weak equations (4) and following standard arguments in finite element analysis yields the discrete finite element equations

$$\mathbf{R}_u = \sum_{e=1}^{n_{\text{elem}}} \int_{\Omega_e^h} \rho \bar{\mathbf{N}}_u^T \mathbf{b} dV + \int_{\partial_t \Omega_e^h} \bar{\mathbf{N}}_u^T \bar{\mathbf{t}} dA - \int_{\Omega_e^h} \bar{\mathbf{B}}_u^T \boldsymbol{\sigma} dV \quad \text{and} \quad \mathbf{R}_\varphi = \sum_{e=1}^{n_{\text{elem}}} \int_{\Omega_e^h} \bar{\mathbf{N}}_\varphi^T \rho^e dV + \int_{\partial_q \Omega_e^h} \bar{\mathbf{N}}_\varphi^T \bar{q} dA + \int_{\Omega_e^h} \bar{\mathbf{B}}_\varphi^T \mathbf{d} dV. \quad (15)$$

Analogous to the continuum setting, the strong discontinuity  $\Gamma_e^h$  is introduced through the local problem requiring in addition to the approximations (14) the approximation of the displacement jumps, the electric potential jumps, the local strain field and the local electric field as

$$[[\mathbf{u}^h]] = \mathbf{J}_u \boldsymbol{\xi}_u, \quad [[\varphi^h]] = \mathbf{J}_\varphi \boldsymbol{\xi}_\varphi, \quad \boldsymbol{\varepsilon}_{\text{local}}^h = \mathcal{C}_u \boldsymbol{\xi}_u \quad \text{and} \quad \mathbf{e}_{\text{local}}^h = -\mathcal{C}_\varphi \boldsymbol{\xi}_\varphi \quad (16)$$

in terms of proper jump interpolation matrices  $\mathbf{J}_u(s)$  and  $\mathbf{J}_\varphi(s)$  depending on a local coordinate  $s$  along the strong discontinuity  $\Gamma_e^h$ , two introduced *compatibility operators*  $\mathcal{C}_u$  and  $\mathcal{C}_\varphi$  as well as two newly introduced internal

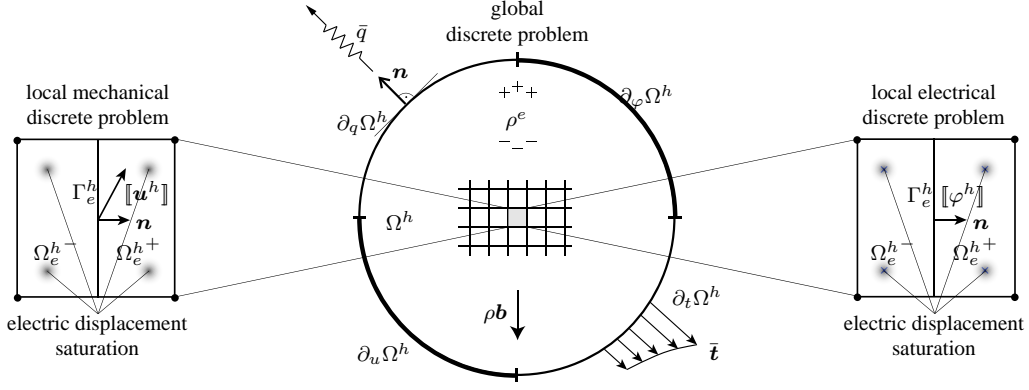


Figure 3: Finite element setting of the finite element approach with embedded strong discontinuities. At the integration points of a single finite element  $\Omega_e^h$  of the global continuum problem the constitutive relation is taking into account electric displacement saturation. Furthermore, the element is able to account for the appearance of a single strong discontinuity  $\Gamma_e^h$  through the local mechanical and electrical problems with possible jumps  $[[\mathbf{u}^h]]$  and  $[[\varphi^h]]$  in the displacement field and the electric potential.

degrees of freedom  $\xi_u$  and  $\xi_\varphi$  holding the mechanical and electrical information of the strong discontinuity, respectively. Combination of (14) and (16) in the presence of a strong discontinuity results in the overall strain and electric fields given as

$$\boldsymbol{\varepsilon}^h = \bar{\mathbf{B}}_u \mathbf{d} + \mathcal{E}_u \xi_u \quad \text{and} \quad \mathbf{e}^h = -\bar{\mathbf{B}}_\varphi \phi - \mathcal{E}_\varphi \xi_\varphi. \quad (17)$$

Insertion of the approximations (17) into the weak form (12) of the required equilibrium along the strong discontinuity then yields the second set of residual equations as

$$\mathbf{r}_u^e = - \int_{\Omega_e^h} \mathcal{E}_u^T \boldsymbol{\sigma} dV - \int_{\Gamma_e^h} \mathbf{J}_u^T \mathbf{t}_\Gamma dA \quad \text{and} \quad \mathbf{r}_\varphi^e = \int_{\Omega_e^h} \mathcal{E}_\varphi^T \mathbf{d} dV - \int_{\Gamma_e^h} \mathbf{J}_\varphi^T q_\Gamma dA \quad (18)$$

where two new quantities, the so called *equilibrium operators*  $\mathcal{E}_u$  and  $\mathcal{E}_\varphi$  are introduced which assure the satisfaction of equilibrium along the strong discontinuity. It is emphasized that the local residual equations (18) only need to be solved for elements  $e$  where a strong discontinuity in the displacements or the electric potential is present. The respective integrals in the bulk and along the strong discontinuity in (18) are easily evaluated with standard quadrature rules of the form

$$\int_{\Omega_e^h} (\cdot) dV = \sum_{l=1}^{n_{\text{quadr}}^{\Omega_e^h}} (\cdot)_l w_l^{\Omega_e^h} j_l \quad \text{and} \quad \int_{\Gamma_e^h} (\cdot) dA = \sum_{l=1}^{n_{\text{quadr}}^{\Gamma_e^h}} (\cdot)_l w_l^{\Gamma_e^h} \ell_{\Gamma_e^h} \quad (19)$$

as summation over the respective quadrature points and account of weights  $w_l^{\Omega_e^h}$  and  $w_l^{\Gamma_e^h}$  in the bulk and along the strong discontinuity as well as the pointwise Jacobian  $j_l$  and the length  $\ell_{\Gamma_e^h}$  of the straight segment  $\Gamma_e^h$ .

A procedure proposed in Linder and Armero (2007) based on the identification of certain mechanical separation modes and in Linder et al. (2011a) based on the identification of certain electrical separation modes of a single finite element allows for the closed form derivation of the compatibility operators introduced in (16) as

$$\begin{aligned} \mathcal{E}_u &= - \left[ \sum_{A \in \Omega_e^{h+}} \bar{\mathbf{B}}_u^A \mathbf{n}, \sum_{A \in \Omega_e^{h+}} \bar{\mathbf{B}}_u^A \mathbf{m}, \sum_{A \in \Omega_e^{h+}} \bar{\mathbf{B}}_u^A (\mathbf{n} \otimes \mathbf{m})^a \bar{\mathbf{x}}_A, \sum_{A \in \Omega_e^{h+}} \bar{\mathbf{B}}_u^A (\mathbf{m} \otimes \mathbf{m}) \bar{\mathbf{x}}_A - (\mathbf{m} \otimes \mathbf{m}) \mathcal{H}_{\Gamma_e^h} \right] \\ \mathcal{E}_\varphi &= - \left[ \sum_{A \in \Omega_e^{h+}} \bar{\mathbf{B}}_\varphi^A, \sum_{A \in \Omega_e^{h+}} s^A \bar{\mathbf{B}}_\varphi^A - \mathbf{m} \mathcal{H}_{\Gamma_e^h} \right] \end{aligned} \quad (20)$$

where  $\mathbf{n}$  and  $\mathbf{m}$  are unit normal and tangential vectors,  $(\mathbf{n} \otimes \mathbf{m})^a = \mathbf{n} \otimes \mathbf{m} - \mathbf{m} \otimes \mathbf{n}$ ,  $\bar{\mathbf{x}}_A = \mathbf{x}_A - \mathbf{x}_\Gamma$  is the vector from the center of the strong discontinuity  $\mathbf{x}_\Gamma$  to a particular node  $A$  of the element and  $\mathcal{H}_{\Gamma_e^h}$  represents the Heaviside function which takes the value 1 in  $\Omega_e^{h+}$  and 0 in  $\Omega_e^{h-}$ .

The equilibrium operators introduced in (18) solely depend on the geometry of the finite element and can be computed in closed form for the mechanical (Linder and Armero, 2007) and the electrical (Linder et al., 2011a)

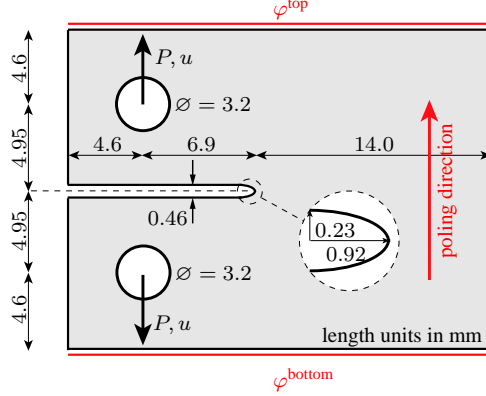


Figure 4: Compact tension test. Geometry and loading illustration of the PZT-4 piezoelectric ceramic plate with a pre-existing horizontal notch. The mechanical load is tensile and applied through circular rigid bars near the bottom and top left corners. Electrically, the plate is loaded by a zero electric potential  $\varphi^{\text{bottom}}$  at the bottom surface and a non-zero electric potential  $\varphi^{\text{top}}$  at the top surface. The poling direction of the specimen is oriented vertically from the bottom to the top surface. Experiments (Park and Sun, 1995b) report a propagating crack from the tip of the notch horizontally towards the right surface.

contribution as

$$\begin{aligned} \mathcal{E}_u &= -\left[ \frac{1}{h_e} \mathbf{p}^{(0)}(\mathbf{n} \otimes \mathbf{n}), \frac{1}{h_e} \mathbf{p}^{(0)}(\mathbf{n} \otimes \mathbf{m})^s, \frac{1}{h_e} \mathbf{p}^{(1)}(\mathbf{n} \otimes \mathbf{n}), \frac{1}{h_e} \mathbf{p}^{(1)}(\mathbf{n} \otimes \mathbf{m})^s \right] \\ \mathcal{E}_\varphi &= -\left[ \frac{1}{h_e} \mathbf{p}^{(0)} \mathbf{n}, \frac{1}{h_e} \mathbf{p}^{(1)} \mathbf{n} \right] \end{aligned} \quad (21)$$

in terms of polynomial functions  $\mathbf{p}^{(k)}(x, y)$  for  $k = 0, 1$  which represent approximations of the products  $\boldsymbol{\sigma} \mathbf{n}$  and  $\mathbf{d} \cdot \mathbf{n}$  of orders up to  $p$  within a local coordinate frame  $\{x, y\}$  centered at the centroid of an element  $\Omega_e^h$  and the measure of the element size  $h_e = A_{\Omega_e^h} / \ell_{\Gamma_e^h}$ . The former can be computed in close form (Linder and Armero, 2007; Linder et al., 2011a) as

$$\mathbf{p}^{(k)}(x, y) = \sum_{i,j=0}^{i+j \leq p} a_{(i,j)}^{(k)} x^i y^j \quad \text{with} \quad [a_{(i,j)}^{(k)}] = \left[ \frac{1}{A_{\Omega_e^h}} \int_{\Omega_e^h} x^{i+m} y^{j+n} dV \right]^{-1} \left[ \frac{1}{\ell_{\Gamma_e^h}} \int_{\Gamma_e^h} s^k x^m y^n dA \right] \quad (22)$$

for all  $m, n = 0, 1, \dots, p$  with  $m+n \leq p$  satisfying the relation between the bulk and the discontinuity integration

$$\frac{1}{A_{\Omega_e^h}} \int_{\Omega_e^h} \mathbf{p}^{(k)}(x, y) x^m y^n dV = \frac{1}{\ell_{\Gamma_e^h}} \int_{\Gamma_e^h} s^k x^m y^n dA. \quad (23)$$

The discrete equations (15) and (18) of the global and the local problem are finally brought to zero through a Newton iterative procedure through which the introduced internal degrees of freedom  $\boldsymbol{\xi}_u$  and  $\boldsymbol{\xi}_\varphi$  can be statically condensed out at the element level (Linder and Armero, 2007; Linder et al., 2011a) leading to an extremely efficient numerical methodology for the simulation of fracture in electromechanical coupled solids.

The electric displacement saturation neither effects the framework of the local problem in the continuum or the finite element setting. What it effects is the constitutive relation at the integration points of the global problem resulting in modified onsets of crack propagation as well as modified crack propagation paths. This dependency is investigated in the following Section 4 and shown to be independent of the chosen finite element discretization. The mechanical as well as the electrical discontinuities are approximated linearly in the following numerical examples.

#### 4 Representative Numerical Simulations

In this section the effect of electric displacement saturation is outlined on two realistic examples for which experimental results are available in Park and Sun (1995b). The goal is to numerically analyze the independence of fracture initiation and subsequent arising crack propagation in piezoelectric ceramics when taking into account electric displacement saturation on the finite element discretization. In Section 4.1 the compact tension test of a PZT-4 piezoelectric ceramics is discussed and in Section 4.2 an off-centered three-point bending test of the same material is simulated.

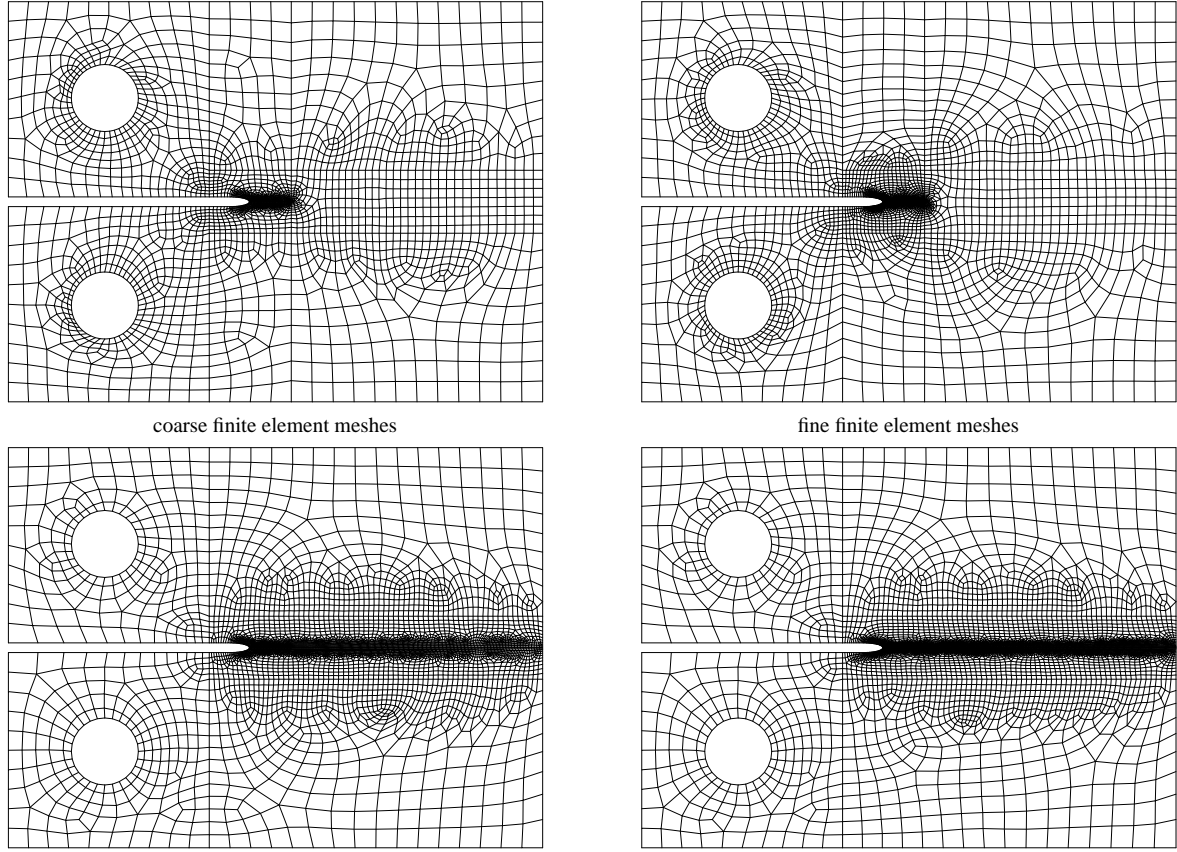


Figure 5: Compact tension test. Illustration of the finite element meshes used for the determination of the electric saturation exponent  $\xi$  (top row) and for the simulations of the propagating crack (bottom row). The meshes for the evaluation of the saturation exponent are only refined at tip of the notch and consist of 3190 Q1 finite elements for the coarse mesh (left) and 5319 Q1 finite elements for the fine mesh (right). The meshes for the simulation of the propagating crack are refined throughout the horizontal region from the tip of the notch towards the right edge and consist of 6159 and 10083 Q1 finite elements for the coarse and the fine mesh, respectively.

#### 4.1 The Compact Tension Test

The first example is provided in the form of a compact tension test made of a plate with a pre-existing notch for which experimental results are given in Park and Sun (1995b). The specimen is 25.5 mm long, 19.1 mm high and has a thickness of 5.1 mm. The horizontal notch is vertically centered and starts from the left surface with a length of 11.5 mm and a thickness of 0.46 mm. The mechanical load puts the plate under tension and is applied in the form of a prescribed vertical displacement through two circular rigid bars with 3.2 mm of diameter placed 4.6 mm from the top and bottom left corners of the plate. Electrically, the specimen which is poled in vertical direction from the bottom to the top surface is loaded by the application of a zero electric potential  $\varphi^{\text{bottom}}$  at the bottom surface and two different non-zero values for the electric potentials  $\varphi^{\text{top}} = -9.55 \text{ kV}$  and  $\varphi^{\text{top}} = -19.1 \text{ kV}$  at the top surface whose values are applied after a short rise time of 0.1  $\mu\text{s}$ . Both, the geometry and the loading of the problem are illustrated in Figure 4.

The material used in the experiment is modeled by the anisotropic constitutive relation provided in Section 2 where the influence of the electric displacement saturation on the determination of crack propagation onset and crack propagation path is investigated. The material parameters are chosen as  $c_{11} = 13.9$ ,  $c_{12} = 7.78$ ,  $c_{13} = 7.43$ ,  $c_{33} = 11.3$  and  $c_{44} = 2.56$  for the elastic constants in units given as  $[10^4 \text{ N/mm}^2]$ , as  $e_{31} = -6.98$ ,  $e_{33} = 13.84$  and  $e_{15} = 13.44$  for the piezoelectric constants in units given as  $[\text{C/m}^2]$  and as  $\epsilon_{11} = 6.0$  and  $\epsilon_{33} = 5.47$  for the dielectric constants in units given as  $[10^{-3} \text{ mC/(kV m)}]$ . The relation between those material parameters and the ones used in Section 2 is given as  $\lambda = c_{12}$ ,  $\mu = (c_{11} - c_{12})/2$ ,  $\alpha_1 = 2c_{44} + c_{12} - c_{11}$ ,  $\alpha_2 = (c_{11} + c_{33})/2 - 2c_{44} - c_{13}$ ,  $\alpha_3 = c_{13} - c_{12}$ ,  $\beta_1 = -e_{31}$ ,  $\beta_2 = -e_{33} + 2e_{15} + e_{31}$ ,  $\beta_3 = -2e_{15}$ ,  $\gamma_1 = -\epsilon_{11}/2$  and  $\gamma_2 = (\epsilon_{11} - \epsilon_{33})/2$ .

With this setup, the experimentally observed propagation of a horizontal crack from the tip of the pre-existing

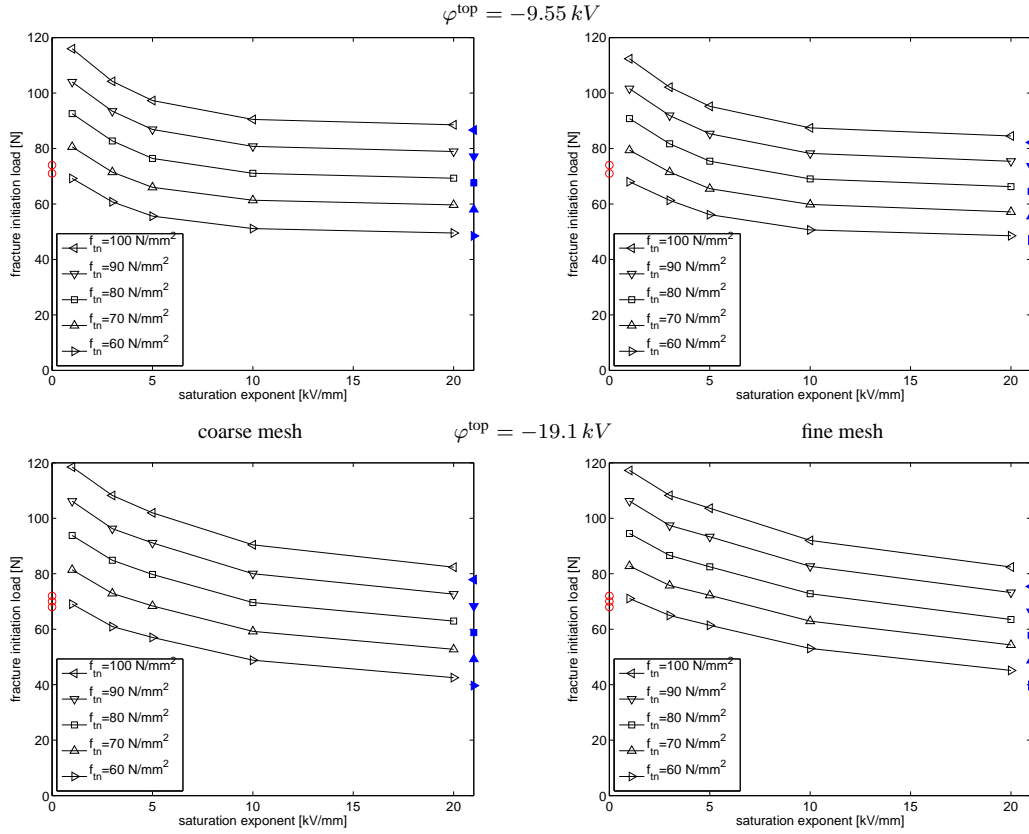


Figure 6: Compact tension test. Influence of the electric saturation parameter  $\xi$  and the tensile normal strength  $f_{t_n}$  on the fracture load of the tension test using a coarse and a fine mesh given in the top row of Figure 5 when loaded for two different values of  $\varphi^{\text{top}}$ . The experimental data are shown by circles, the values for  $\xi \rightarrow \infty$  (corresponding to the case without electric displacement saturation) are shown by filled markers for the different tensile strengths.

notch towards the right surface shall be simulated. Since the main goal of this work is to show the independence of the electric displacement saturation model of exponential type and its influence on the crack initiation and crack propagation on the finite element discretization, different finite element meshes are used in the numerical simulations presented below. The meshes illustrated in the top row of Figure 5 consist of a coarse and a fine mesh, both refined at the crack tip, made up by 3190 and 5319 Q1 elements, respectively. The meshes illustrated in the bottom row of Figure 5 consist of a coarse and a fine mesh made up by 6159 and 10083 Q1 finite elements which are refined at the region from the tip of the pre-existing notch towards the right surface representing the region where the crack path is expected based on the experimental results reported in Park and Sun (1995b). It is noted that rather than enforcing the crack to propagate along the finite element edges, the proposed formulation allows the crack to propagate through the individual finite elements.

Before targeting the simulation of the actual crack propagation, the introduced saturation exponent  $\xi$  in (7) of the electric displacement saturation model needs to be evaluated. To do so, the two meshes which are refined around the region of the tip of the pre-existing notch in the top row of Figure 5 are used when loaded with  $\varphi^{\text{top}} = -9.55 \text{ kV}$  and  $\varphi^{\text{top}} = -19.1 \text{ kV}$ . The saturation exponent is varied from  $\xi \rightarrow \infty$ , which corresponds to the case when no electric displacement saturation is accounted for, to  $\xi = 1 \text{ kV/mm}$  which results in a large electric saturation zone at the tip of the pre-existing notch. Secondly, the tensile strength of the material is varied from  $f_{t_n} = 60 - 100 \text{ N/mm}^2$ . With these values the crack propagation onset given by the numerical solution for the two different applied electric potentials at the top surface is computed and compared with the experimental results. In Linder and Miehe (2012) the same procedure is applied only for the coarse mesh which resulted in the best fitting for parameters of  $\xi = 10 \text{ kV/mm}$  and  $f_{t_n} = 80 \text{ N/mm}^2$  as shown in the left column of Figure 6. Based on the coinciding results obtained for the fine mesh, illustrated in the right column of Figure 6, the mesh insensitivity of the determination of the electric saturation exponent is clearly demonstrated. Furthermore, the result for the tensile strength is close to the experimentally used value of  $75.8 \text{ N/mm}^2$  reported in Park (1994).

Next, the actual crack propagation when applying an electric potential at the top surface of  $\varphi^{\text{top}} = -9.55 \text{ kV}$  is modeled using the two meshes in the bottom row of Figure 5 and the above obtained values for the saturation

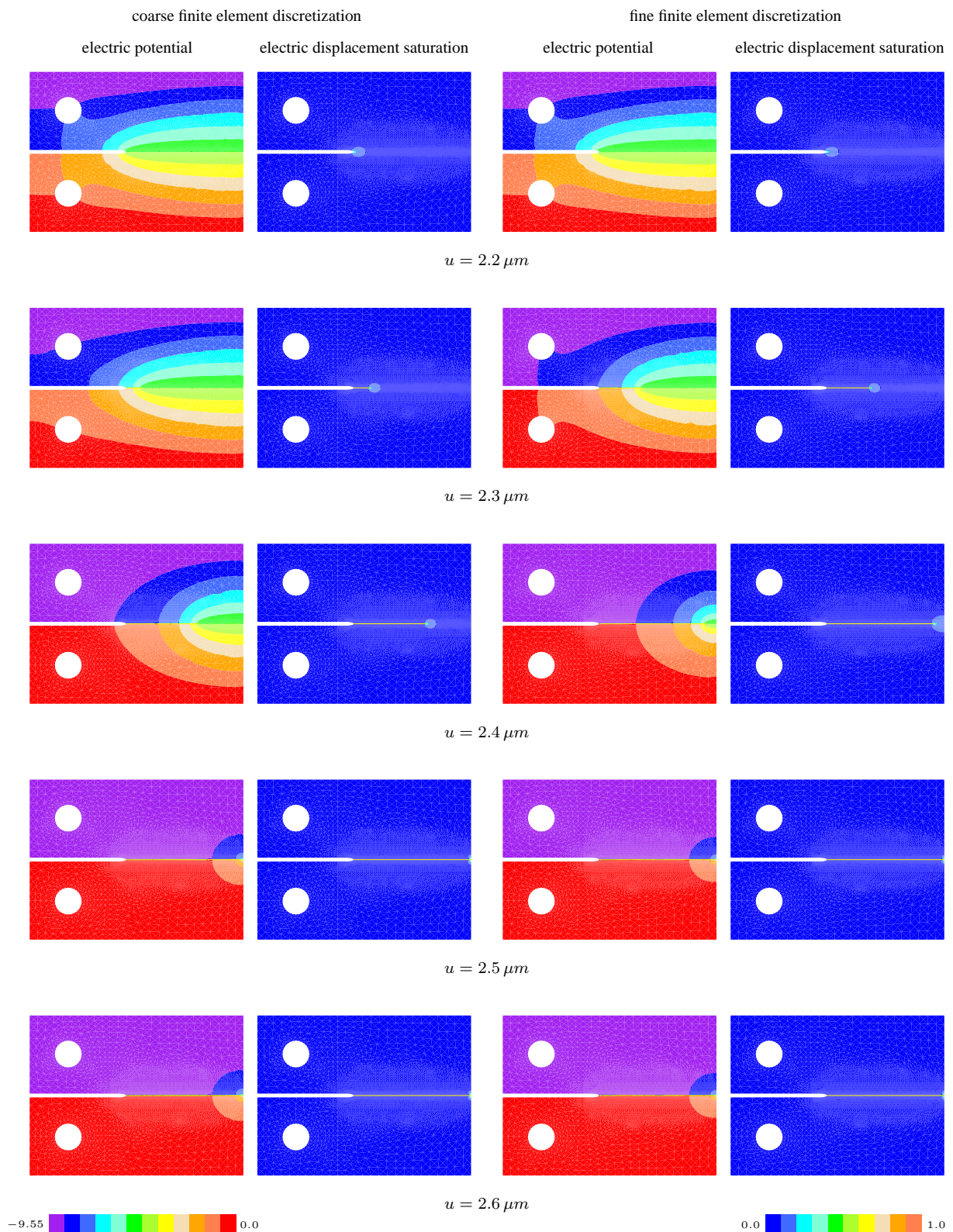


Figure 7: Compact tension test. Influence of the finite element discretization on the crack propagation which is shown as yellow line using the coarse and fine mesh of the bottom row of Figure 5 for an active electric displacement saturation with a saturation exponent of  $\xi = 10 \text{ kV/mm}$ . Shown is the evolution of the electric potential and the zone of electric displacement saturation by plotting the value  $1 - \exp(-|I_6|/\xi)$ . The latter is observed to be small and travels along with the propagating crack tip.

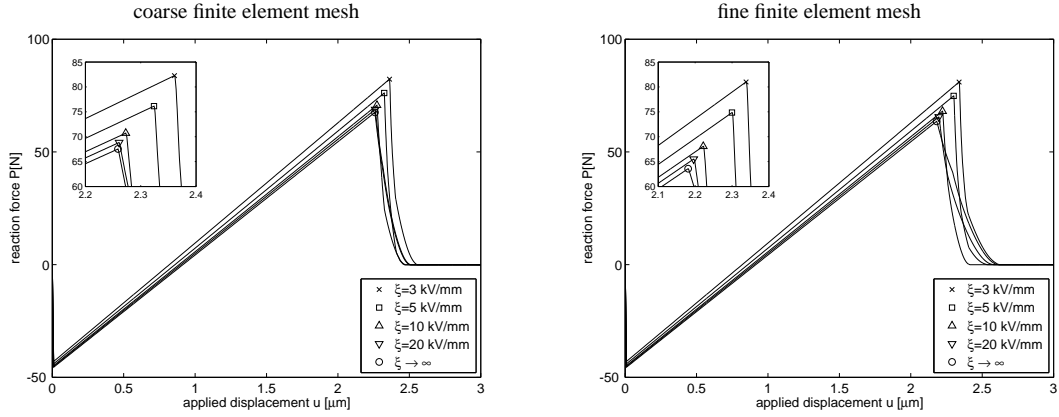


Figure 8: Compact tension test. Influence of the finite element discretization on the relation between the reaction force and the applied displacement using the coarse (left) and the fine (right) finite element mesh shown in the bottom row of Figure 5 and for different saturation exponents  $\xi = 3, 5, 10, 20, \infty \text{ kV/mm}$ . For both discretizations a smaller value of  $\xi$  results in a larger electric displacement saturation zone, a higher reaction force at which the specimen fractures and a faster propagating crack from the tip of the pre-existing notch towards the right surface.

exponent and the tensile strength of the material. The goal is to show that both, the onset of crack propagation as well as the crack propagation itself is independent of the two chosen finite element discretizations. The results obtained for the coarse mesh, also reported in Linder and Miehe (2012), shown in the left column of Figure 7 are supported by the results obtained for the fine finite element discretization shown in the right column of Figure 7 with an almost identical behavior of the crack propagation simulation which again demonstrates the mesh independency of the proposed formulation. Also the size of the electric saturation zone, illustrated in Figure 7 by plotting the value  $1 - \exp(-|I_6|/\xi)$ , which is 0 when no saturation takes place and 1 when the material is electrically fully saturated, is in close agreement for both discretizations and travels together with the crack tip towards the right surface.

Finally, the mesh size independency is also outlined through an evaluation of the reaction force versus applied displacement relation for the two meshes in the bottom row of Figure 5 when applying an electric potential  $\varphi^{\text{top}} = -9.55 \text{ kV}$  at the top surface. The results are shown in Figure 8 which agree for both discretizations in the sense that smaller values of  $\xi$ , characteristic for larger electric displacement saturation zones, result in an increase of the initiation load of fracture and a subsequent faster decay showing a faster crack propagation speed.

## 4.2 The off-centered Three Point Bending Test

The second example for which the influence of finite element discretization is investigated is the off-centered three point bending test for which experimental results are again provided in Park and Sun (1995b). It consists of a plate  $19.1 \text{ mm}$  in length,  $9 \text{ mm}$  in height and with a thickness of again  $5.1 \text{ mm}$ . The pre-existing vertical notch has a length of  $4 \text{ mm}$ , is  $0.46 \text{ mm}$  thick and shifted  $4 \text{ mm}$  to the right of the horizontal center of the plate. Mechanically, the specimen is loaded by an imposed displacement at the center of the top surface. The electrical loading is given by the application of a zero electric potential  $\varphi^{\text{left}}$  at the left surface and a non-zero electric potential  $\varphi^{\text{right}} = -9.55 \text{ kV}$ , applied after a short rise time of  $0.1 \mu\text{s}$  at the right surface. The poling direction of the specimen is horizontal and points from the left towards the right. Both, the geometry and the loading of the problem are illustrated in Figure 9. The material parameters are the same as those for the compact tension test in Section 4.1 together with the same values used for the fitted parameters of the tensile strength  $f_{t_n}$  and the saturation exponent  $\xi$ .

The two chosen finite element discretizations, both refined in the region where the crack is supposed to propagate, consist of 1506 and 2692 Q1 elements and are illustrated in Figure 10. Expected is a crack onset at the tip of the pre-existing notch with a subsequent initially vertical but then curved propagation in the direction of the point where the mechanical load is applied. The observed vertical initial region in the crack path is shown in Linder and Miehe (2012) to be amplified in the presence of electric displacement saturation when using the coarse finite element discretization. It remains to be shown that the same tendency is obtained for the fine finite element discretization. The results of the size of the electric saturation zone obtained by plotting the value  $1 - \exp(-|I_6|/\xi)$  within the range  $[0, 0.5]$  and the crack propagation path is illustrated in Figure 11 and demonstrates again the mesh size

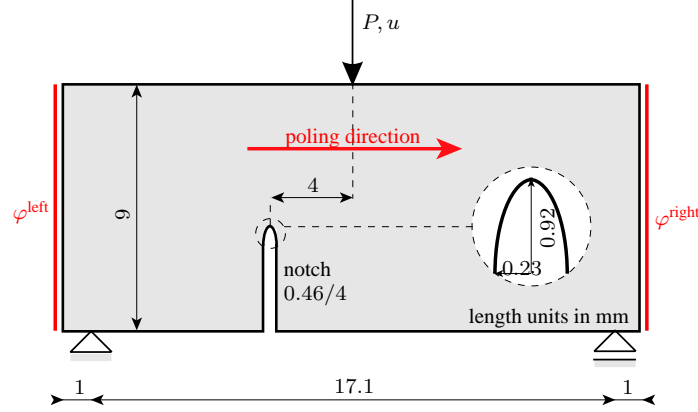


Figure 9: Off-centered three point bending test. Geometry and loading illustration of the PZT-4 piezoelectric ceramic plate with a pre-existing off-centered vertical notch. The mechanical loading is given by an imposed displacement at the center of the top surface. The electrical loading is applied in the form of a zero electric potential  $\varphi^{\text{left}}$  at the left surface and a non-zero electric potential  $\varphi^{\text{right}}$  at the right surface. The poling direction of the specimen is oriented horizontal from the left towards the right surface. Experiments (Park and Sun, 1995b) report an initial vertical crack initiating from the tip of the pre-existing notch which is subsequently curved towards the point where the mechanical load is applied.

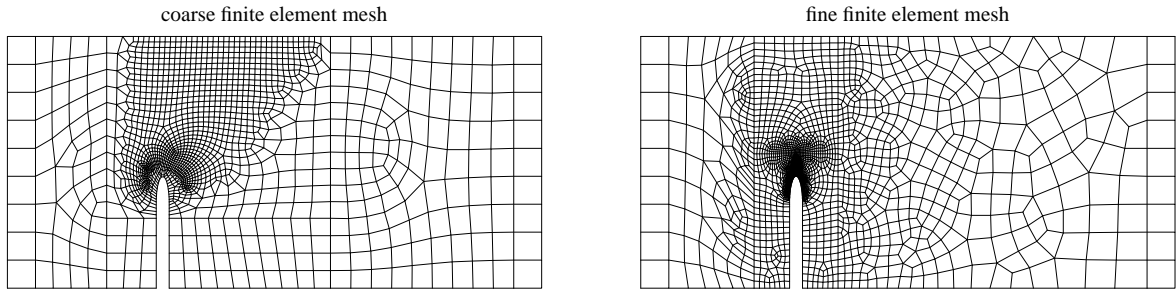


Figure 10: Off-centered three point bending test. Illustration of the coarse (left) and fine (right) finite element meshes consisting of 1506 and 2692 Q1 finite elements, respectively. Both meshes are refined in the region where the crack is supposed to propagate.

insensitivity of the model. It can be observed, that the orientation of the electric saturation zone is normal to the horizontal poling direction rather than tangential to the crack path orientation which is in line with the originally proposed strip saturation model of Gao et al. (1997). It can be further seen that the crack advances earlier for the coarse mesh but the final result of the crack path remains mesh independent.

Finally, in Figure 12 a comparison of the obtained crack propagation paths for the two finite element discretizations outlined in Figure 10 with the experimental results reported in Park (1994) and Park and Sun (1995b) is made for different values of the saturation exponent  $\xi = 3, 5, 10, 20, \infty \text{ kV/mm}$ . Comparing the results for the coarse (left column) and fine (right column) finite element discretization demonstrated again the mesh independency of the method. Both meshes show that a smaller saturation exponent (characterizing a larger electric displacement saturation zone) leads to a more distinct vertical orientation of the crack path. A very good agreement with the experimental results is obtained for both meshes when the saturation exponent is chosen as  $\xi = 10 \text{ kV/mm}$  which is in line with the results obtained by the parameter fitting of Section 4.1 for the compact tension test.

To conclude this section, the electric displacement saturation model of exponential type proposed in Linder and Miehe (2012) is shown to predict the crack propagation onset as well as the crack propagation path independent of the chosen finite element discretization. This assertion is drawn based on numerical simulations of two notched PZT-4 piezoelectric ceramic specimens and comparison of the obtained numerical results with the experimental results reported in Park and Sun (1995b).

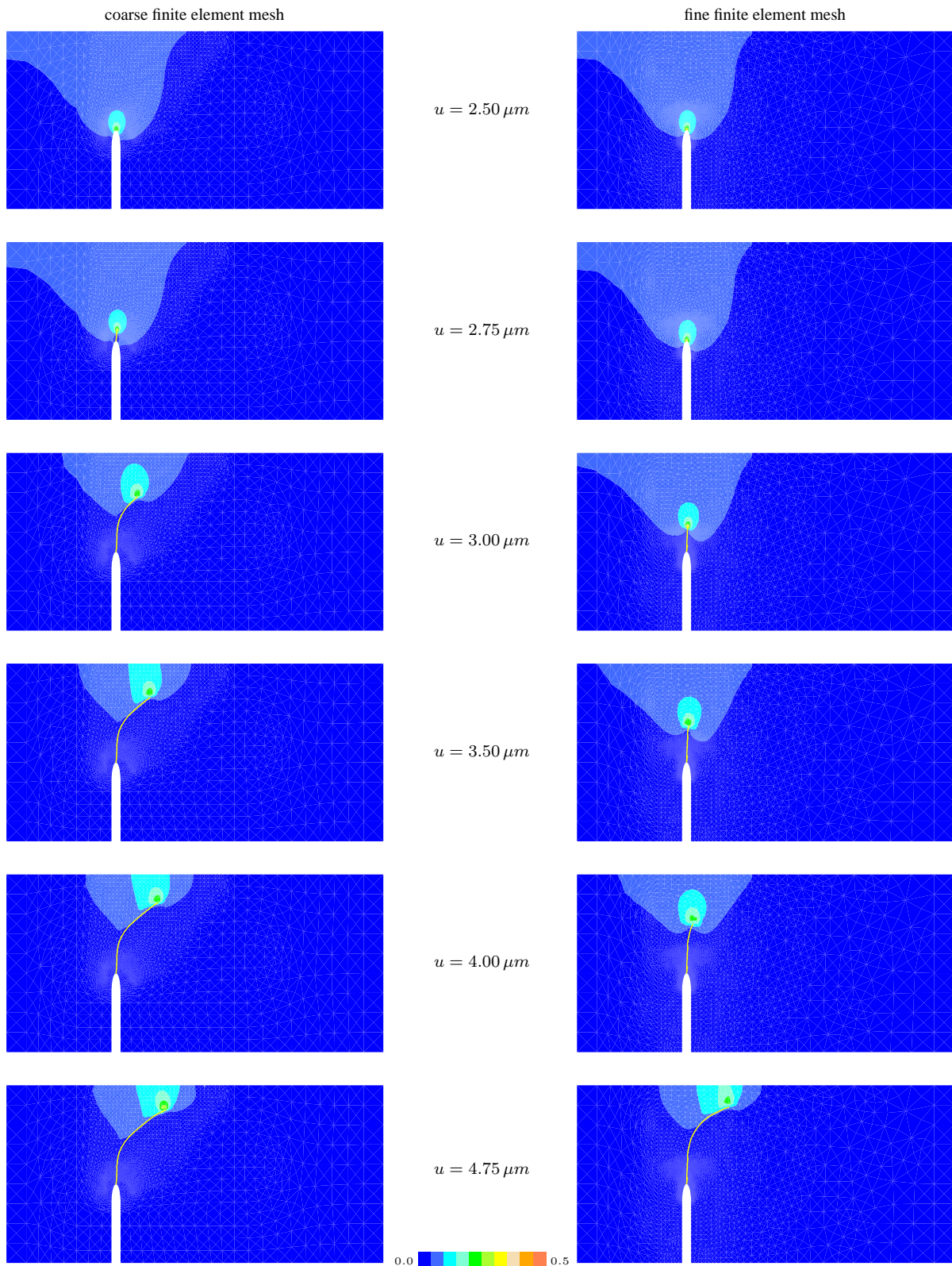


Figure 11: Off-centered three point bending test. Influence of the finite element discretization on the crack propagation which is shown as yellow line using the coarse (left column) and fine (right column) mesh shown in Figure 10 for an active electric displacement saturation using a saturation exponent of  $\xi = 10 \text{ kV/mm}$ . The value  $1 - \exp(-|I_6|/\xi)$  is used to illustrate the electric saturation zone which is propagation along with the advancing crack tip. The crack starts to propagate earlier for the coarse mesh but the final crack paths are mesh independent.

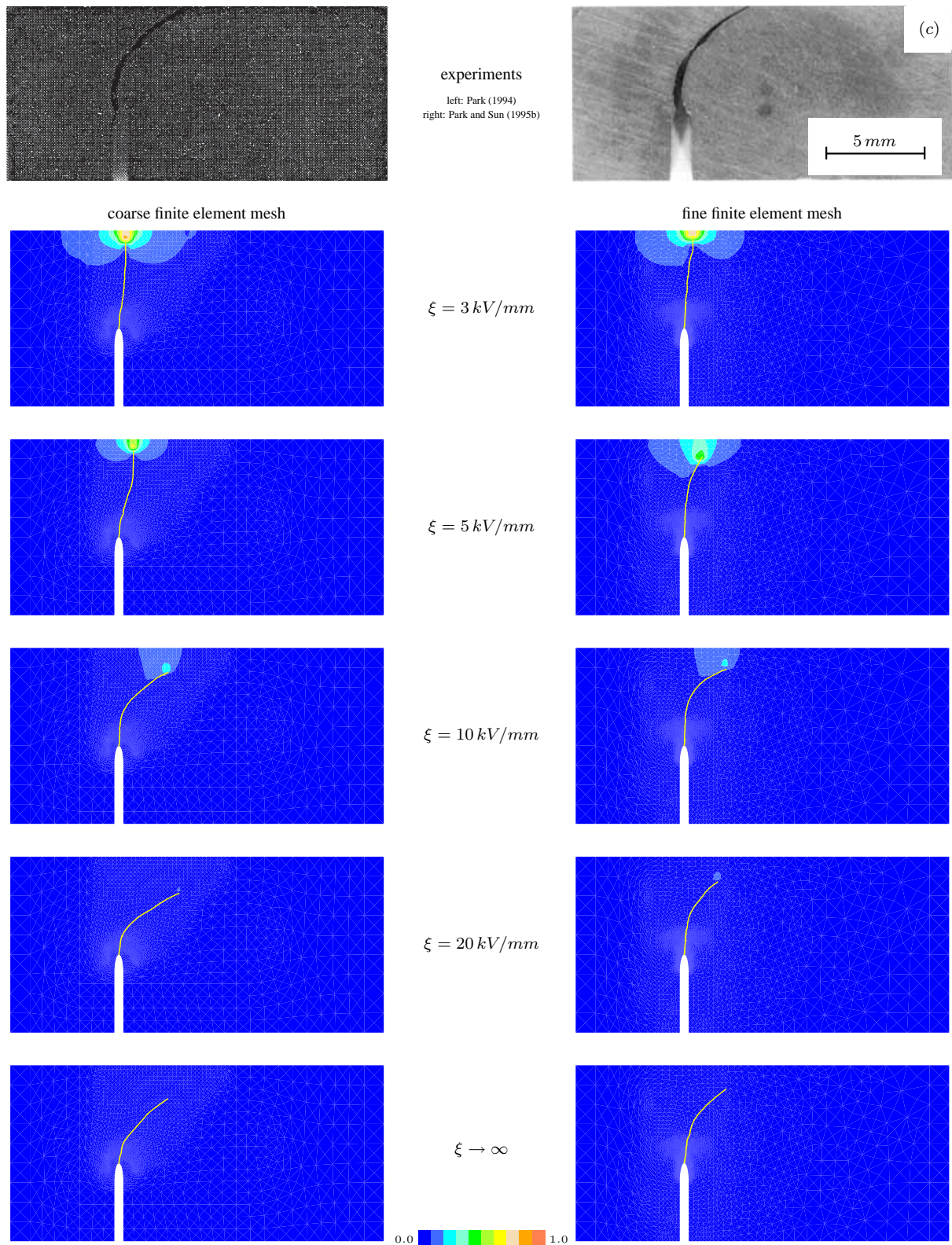


Figure 12: Off-centered three point bending test. Influence of the finite element discretization on the final crack path for different values of the saturation exponent  $\xi = 3, 5, 10, 20, \infty \text{ kV/mm}$ . The result for the coarse mesh is shown in the left column whereas the result of the fine mesh is shown in the right column. Both discretizations show that a smaller value of the saturation exponent results in a more vertical crack path. Whereas too small values of  $\xi$  result in non-physical crack paths, the choice of  $\xi = 10 \text{ kV/mm}$  is in good agreement with the experimentally observed crack path for both discretizations.

## 5 Conclusion

In this work the effect of electric displacement saturation of exponential type on the determination of the onset of crack propagation as well as on the resulting crack propagation paths in fracturing piezoelectric ceramics proposed in Linder and Miehe (2012) is analyzed from a numerical point of view. It is numerically shown that the conclusions drawn in the work of Linder and Miehe (2012) with regard to the effect of electric displacement saturation are independent of the finite element discretization. The determination of the saturation exponent through the compact tension test is revealed to be independent of the mesh size as are the obtained onsets and crack propagation paths for the compact tension and the off-centered three point bending test. The numerically obtained curved crack paths in the latter test, for the first time obtained in Linder and Miehe (2012), are reproduced for a much finer discretization in this work. In the future, similar phenomena as the electric displacement saturation influencing the fracture behavior of electromechanical coupled materials are being analyzed for materials with inherent microstructure like in our recently proposed model of the viscous behavior in polymers (Linder et al., 2011b).

**Acknowledgments.** Financial support for this research was provided by the German Research Foundation (DFG) under Grant No. Li 1915/1-1 and the Cluster of Excellence in Simulation Technology (ExC 310/1) at the University of Stuttgart. This support is gratefully acknowledged.

## References

- Armero, F.; Garikipati, K.: Recent advances in the analysis and numerical simulation of strain localization in in-elastic solids. In: *Computational Plasticity Fundamentals and Applications*, pages 547–561, Barcelona (1995).
- Armero, F.; Garikipati, K.: An analysis of strong discontinuities in multiplicative finite strain plasticity and their relation with the numerical simulation of strain localization in solids. *Int. J. Solids Struct.*, 33, (1996), 2863–2885.
- Armero, F.; Linder, C.: New finite elements with embedded strong discontinuities in the finite deformation range. *Comput. Methods Appl. Mech. Engrg.*, 197, (2008), 3138–3170.
- Armero, F.; Linder, C.: Numerical simulation of dynamic fracture using finite elements with embedded discontinuities. *Int. J. Fract. Mech.*, 160, (2009), 119–141.
- Barnett, D. M.; Lothe, J.: Dislocations and line charges in anisotropic piezoelectric insulators. *Physica Status Solidi (B)*, 67, (1975), 105–111.
- Deeg, W. F. J.: *The analysis of dislocation, crack, and inclusion problems in piezoelectric solids*. Ph.D. thesis, Stanford University (1980).
- Dugdale, D. S.: Yielding of steel sheets containing slits. *J. Mech. Phys. Solids*, 8, (1960), 100–104.
- Eshelby, J. D.; Read, W. T.; Shockley, W.: Anisotropic elasticity with applications to dislocation theory. *Acta Metall.*, 1, (1953), 251–259.
- Fu, R.; Zhang, T. Y.: Effects of an electric field on the fracture toughness of poled lead zirconate titanate ceramics. *J. Am. Ceram. Soc.*, 83, (2000), 1215–1218.
- Fulton, C. C.; Gao, H.: Effect of local polarization switching on piezoelectric fracture. *J. Mech. Phys. Solids*, 49, (2001), 927–952.
- Gao, H.; Zhang, T. Y.; Tong, P.: Local and global energy release rates for an electrically yielded crack in a piezoelectric ceramic. *J. Mech. Phys. Solids*, 45, (1997), 491–510.
- Hao, T. H.; Shen, Z. Y.: A new electric boundary condition of electric fracture mechanics and its applications. *Eng. Fract. Mech.*, 47, (1994), 793–802.
- Jona, F.; Shirane, G.: *Ferroelectric crystals*, vol. 1. Dover Publications (1993).
- Landis, C. M.: Energetically consistent boundary conditions for electromechanical fracture. *Int. J. Solids Struct.*, 41, (2004), 6291–6315.
- Lekhnitskii, S. G.: *Theory of Elasticity of an anisotropic elastic body*. Gostekhizdat, Moscow (1950).

- Linder, C.; Armero, F.: Finite elements with embedded strong discontinuities for the modeling of failure in solids. *Int. J. Numer. Methods Engrg.*, 72, (2007), 1391–1433.
- Linder, C.; Armero, F.: Finite elements with embedded branching. *Finite Elem. Anal. Des.*, 45, (2009), 280–293.
- Linder, C.; Miehe, C.: Effect of electric displacement saturation on the hysteretic behavior of ferroelectric ceramics and the initiation and propagation of cracks in piezoelectric ceramics. *J. Mech. Phys. Solids*, 60, (2012), 882–903.
- Linder, C.; Rosato, D.; Miehe, C.: New finite elements with embedded strong discontinuities for the modeling of failure in electromechanical coupled solids. *Comput. Methods Appl. Mech. Engrg.*, 200, (2011a), 141–161.
- Linder, C.; Tkachuk, M.; Miehe, C.: A micromechanically motivated diffusion-based transient network model and its incorporation into finite rubber viscoelasticity. *J. Mech. Phys. Solids*, 59, (2011b), 2134–2156.
- McMeeking, R. M.: Towards a fracture mechanics for brittle piezoelectric and dielectric materials. *Int. J. Fract. Mech.*, 108, (2001), 25–41.
- Miehe, C.; Rosato, D.: A rate-dependent incremental variational formulation of ferroelectricity. *Int. J. Eng. Sci.*, 49, (2011), 466–496.
- Moës, N.; Dolbow, J.; Belytschko, T.: A finite element method for crack growth without remeshing. *Int. J. Numer. Methods Engrg.*, 46, (1999), 131–150.
- Mosler, J.; Meschke, G.: 3D modelling of strong discontinuities in elastoplastic solids: fixed and rotating localization formulations. *Int. J. Numer. Methods Engrg.*, 57, (2003), 1553–1576.
- Oliver, J.; Huespe, A. E.; Pulido, M. D. G.; Samaniego, E.: On the strong discontinuity approach in finite deformation settings. *Int. J. Numer. Methods Engrg.*, 56, (2003), 1051–1082.
- Pak, Y. E.: Crack extension force in a piezoelectric material. *J. Appl. Mech.*, 57, (1990), 647–653.
- Park, S.: *Fracture behavior of piezoelectric materials*. Ph.D. thesis, Purdue University (1994).
- Park, S.; Sun, C. T.: Effect of electric field on fracture of piezoelectric ceramics. *Int. J. Fract. Mech.*, 70, (1995a), 203–216.
- Park, S.; Sun, C. T.: Fracture criteria for piezoelectric ceramics. *J. Am. Ceram. Soc.*, 78, (1995b), 1475–1480.
- Parton, V. Z.: Fracture mechanics of piezoelectric materials. *Acta Astronaut.*, 3, (1976), 671–683.
- Schröder, J.; Gross, D.: Invariant formulation of the electromechanical enthalpy function of transversely isotropic piezoelectric materials. *Arch. Appl. Mech.*, 73, (2004), 533–552.
- Simo, J.; Oliver, J.: A new approach to the analysis and simulation of strong discontinuities. In: Z. Bažant; Z. Bittnar; M. Jirasek; J. Mazars, eds., *Fracture and damage in quasibrittle structures*, vol. 2–6, pages 25–39 (1994).
- Simo, J. C.; Oliver, J.; Armero, F.: An analysis of strong discontinuities induced by strain-softening in rate-independent inelastic solids. *Comput. Mech.*, 12, (1993), 277–296.
- Stroh, A. N.: Dislocations and cracks in anisotropic elasticity. *Philos. Mag.*, 3, (1958), 625–646.
- Suo, Z.; Kuo, C. M.; Barnett, D. M.; Willis, J. R.: Fracture mechanics for piezoelectric ceramics. *J. Mech. Phys. Solids*, 40, (1992), 739–765.
- Tobin, A. G.; Pak, Y. E.: Effect of electric fields on fracture behavior of PZT ceramics. In: V. K. Varadan, ed., *Proceedings of SPIE, Smart Struct. Mater.*, vol. 78, pages 78–86 (1993).
- Wang, H.; Singh, R. N.: Crack propagation in piezoelectric ceramics: Effects of applied electric fields. *J. Appl. Phys.*, 81, (1997), 7471–7479.
- Wells, G. N.: *Discontinuous modelling of strain localisation*. Ph.D. thesis, Technical University Delft (2001).

---

Address: Jun.-Prof. Christian Linder, Ph.D., Institute of Applied Mechanics (CE) Chair I, University of Stuttgart, 70550 Stuttgart, Pfaffenwaldring 7, Germany.  
 email: linder@mechbau.uni-stuttgart.de